

Stability and angiotensin converting enzyme inhibitory activity of peptide RVPSL-loaded graphene oxide

¹Yu, Z., ^{1,2}Guo, H., ^{1,2*}Zhao, W., ³Zhang, M., ^{1,2}Li, J. and ⁴Liu, J.

¹College of Food Science and Engineering, Bohai University, Jinzhou 121013, P.R. China

²National and Local Joint Engineering Research Centre of Storage, Processing and Safety Control Technology for Fresh Agricultural and Aquatic Products, Bohai University, Jinzhou 121013, P.R. China

³College of Life Science and Technology, Xinjiang University, Urumqi 830046, P.R. China

⁴Laboratory of Nutrition and Functional Food, Jilin University, Changchun 130062, P.R. China

Article history

Received: 5 March 2020
Received in revised form:
19 July 2020
Accepted:
5 October 2020

Abstract

Previous work has demonstrated that the angiotensin converting enzyme (ACE) inhibitory peptide RVPSL is very unstable and loses its ACE inhibitory activity in the gastrointestinal tract. Thus, graphene oxide (GO) was used to improve the stability of RVPSL in the present work. The structure and morphology of RVPSL-GO were characterised using Fourier transform-infrared spectroscopy, X-ray photoelectron spectroscopy, scanning electron microscopy, and atomic force microscopy. Moreover, the cytotoxicity of RVPSL-GO was examined using HepG2 cells. RVPSL was successfully covalently bonded to GO and the RVPSL-loading capacities of RVPSL-GO were calculated to be 1.05 mg RVPSL/mg GO, and the loading efficiency value was 95.02%. The results showed that GO enhanced RVPSL ACE activity (at 0.026 mg/mL) from 26.47 to 39.70%. This may have caused a higher local concentration of RVPSL in the solution after GO was modified. Moreover, the stability of RVPSL was improved with protection from GO. The ACE inhibition rate of RVPSL-GO was 49.08%, while RVPSL was completely degraded after 2 h in simulated gastrointestinal digestion. In addition, RVPSL-GO displayed high viability for HepG2 cells with no significant cytotoxicity.

© All Rights Reserved

Keywords

peptide,
modification,
stability,
angiotensin converting
enzyme,
protection

Introduction

Peptides have unique potent bioactivities to treat diseases owing to their selective and excellent safety profile (Tsomaia, 2015; Ouberai *et al.*, 2017). It has been reported that bioactive peptides are unstable in the gastrointestinal tract (GI) (Wang *et al.*, 2015) where they can be degraded by local proteases (Han *et al.*, 2019; Zhao *et al.*, 2020). Therefore, there has been increased interest in developing ways to overcome this obstacle. Many methods are available to stabilise active peptide conformations, including stapling (Schafmeister *et al.*, 2000; Shim *et al.*, 2013), hydrogen bond surrogates (Cabezas and Satterthwait, 1999), beta-hairpin mimetics (Fasan *et al.*, 2004), and macrocyclisation (Villar *et al.*, 2014). Nano-material has provided favourable ways to protect, deliver, and control the release of compounds (Ainslie *et al.*, 2009; Martins *et al.*, 2018; Li *et al.*, 2019). Utilising various peptides to modify the surface of nano-material has successfully achieved cell-specific targeting (Hu *et al.*, 2016).

Graphene oxide (GO) contains aromatic

regions randomly interspersed with oxidised aliphatic rings. These oxidised rings contain a mass of epoxide (C-O-C) and hydroxyl (C-OH) groups. Carbonyl (C=O) and carboxylic acid (-COOH) groups are also detected on the edge of GO. GO easily disperses in water and other organic solvents due to oxygen functional groups (Stankovich *et al.*, 2006). These advantages promote its application in the field of biology. As compared to other carbon materials, such as fullerenes and carbon nanotubes, GO is a low-priced raw material that is simple to synthesise at a controllable size. In addition, GO also has good hydrophilicity and high specific surface area (Hirata *et al.*, 2005; Szabó *et al.*, 2006) which is also an attractive material for biomedical applications due to its unique properties, such as the abundance of surface polar groups, amphiphilicity, and biocompatibility.

Numerous peptides purified from food protein hydrolysates have been considered as the functional ingredients to promote human health (Yu *et al.*, 2018). Absorption is the basis for peptides to exert their bioactivities, and low absorption is a problem with applications of some bioactive peptides. Our previous

*Corresponding author.
Email: zhaowenzhu777@163.com

work has demonstrated that the peptide RVPSL exhibits angiotensin converting enzyme (ACE)-inhibitory activity with an IC_{50} value of 20 μ M (Yu *et al.*, 2011). Moreover, RVPSL in a range of 5 - 50 mg/kg exerts an anxiolytic effect on spontaneous hypertensive rats, so it could be considered a possible functional food or food ingredient (Yu *et al.*, 2016). However, RVPSL is unstable in human GI tract because of the degradation by digestive enzymes and plasma peptidases, and low absorption through the intestinal barrier (Vermeirssen *et al.*, 2004).

In the present work, GO nanomaterial was used as a carrier to load the peptide RVPSL using the EDCI/NHS coupling group. Then, the structure and morphology of RVPSL-GO were characterised to ensure whether peptide RVPSL bonded to GO using UV-vis spectrophotometry, Fourier transform-infrared spectroscopy (FT-IR), X-ray powder diffraction (XRD), X-ray photoelectron spectroscopy (XPS), scanning electron microscopy (SEM), and atomic force microscopy (AFM). Subsequently, the ACE-inhibitory activity of RVPSL-GO was measured, and GI digestion was simulated to determine the stability of RVPSL-GO. The cytotoxicity of RVPSL-GO was also assessed.

Materials and methods

Reagents and materials

ACE (protease from rabbit lungs) and hippuryl-histidyl-leucine were purchased from Sigma-Aldrich Co. (St. Louis, MO, USA). Trifluoroacetic acid, acetonitrile, and methanol were purchased from Fisher Scientific Co. (Waltham, MA, USA). Pepsin (1:10,000) and trypsin (1:250) were purchased from Solarbio (Beijing, China). All other reagents and chemicals used were of analytical grade. The peptide RVPSL was synthesized by Shanghai Top-peptide Co. Ltd. (Shanghai, China).

Synthesis of RVPSL-GO

GO was fabricated following the modified Hummers method (Szabó *et al.*, 2006), and the ACE-inhibitory peptide RVPSL was attached to GO through a coupling reaction. To attach RVPSL to GO, the carboxylic acid (-COOH) group of GO was modified with EDCI and NHS. First, 2 mg GO was added to 20 mL distilled water, and the solution was sonicated for 2 h. Then, 10 mg EDCI and 20 mg NHS were added to the solution. The reaction mixture was stirred at 37°C for 5 min. Next, 2.2 mg RVPSL was added followed by ultrasound for 10 min. The mixture was stirred at 37°C for 6 h so that the RVPSL amines could completely combine with the GO carboxylic

acid groups. The suspension was centrifuged, and the supernatant (S-RVPSL) was concentrated to determine the rate of RVPSL bonded to GO. The peptide RVPSL-loading capacities (LC) and loading efficiencies (LE) were estimated using Eqs. 1 and 2, respectively, as follows:

$$LC\left(\frac{\text{mg}}{\text{mg}}\right) = \frac{\text{Mass of loading RVPSL (mg)}}{\text{Mass of applied GO (mg)}} \quad (\text{Eq. 1})$$

$$LE(\%) = \frac{\text{Mass of loading RVPSL (mg)}}{\text{Total mass of applied RVPSL (mg)}} \times 100\% \quad (\text{Eq. 2})$$

The precipitate was washed three times with distilled water and freeze-dried. Finally, the powder was the ACE functionalised carboxylic acid-modified GO.

Characterisation of RVPSL-GO

The GO and RVPSL functional graphene oxide (RVPSL-GO) dispersion was characterised by UV-Vis spectroscopy to ensure that the GO powder was dispersed perfectly. Briefly, 1 mg GO was dispersed in distilled water (10 mL), followed by 30 min of ultrasound to obtain the dispersed solution at a wavelength of 200 - 800 nm. GO and RVPSL-GO were confirmed by FT-IR. The dispersion of the samples was placed in evaporated dishes, dried at room temperature, and evaluated in the range of 4000 - 400 cm^{-1} . GO and RVPSL-GO were pre-treated, dried at room temperature, and ground into a powder. XRD was used to characterise of the samples with Cu-K α radiation ($\lambda = 0.154$ nm), tube pressure of 40 Kv, pipe flow value of 40 mA, and a 2θ range of 10 - 60°. D-spacing of each type of GO and RVPSL-GO was calculated using Bragg's in Eq. 3:

$$n\lambda = 2d\sin(\theta) \quad (\text{Eq. 3})$$

where, n = positive integer, λ = wavelength of the incident wave, and θ = diffraction angle.

The chemical composition of GO and RVPSL-GO was determined by XPS. The XPS spectra were taken using a Thermo ESCALAB 250 with an Al anode (K-alpha radiation; 150 W X-ray excitation source) in the constant analyser energy mode (29.35 eV pass energy). The dried GO and RVPSL-GO powder were immobilised on a copper sheet. Surface morphology was observed and photographed after a platinum spray treatment. SEM images were obtained. GO and RVPSL-GO (1 mg) were added to 10 mL distilled water, respectively. A suspension was obtained after 10 min of sonication. Next, 10 μ L of the solution was dropped on the surface of fresh mica

tablets, dried at room temperature, and detected by AFM.

In vitro ACE-inhibitory activity assay

ACE-inhibitory activity was measured followed by high-performance liquid chromatography following a method reported previously (Yu *et al.*, 2019).

Simulated gastrointestinal digestion

RVPSL-GO was subjected to simulated GI digestion according to a method described previously (Guarnieri *et al.*, 2018). The RVPSL-GO solution (2 mL, the RVPSL concentration was 0.105 mg/mL) was digested with simulated gastric fluid (prepared with pepsin, pH 1.2) at 1:100 (w/v), at 37°C for 1, 2, and 4 h. Then, the pH of the solution was adjusted to 6.8 with 1 mol/L NaOH, and the same volume of intestinal digest (prepared with trypsin, pH 6.8) at 1:100 (w/v) was added for 1, 2, and 4 h. The mixture solution was boiled in water for 10 min to terminate digestion. After cooling down to room temperature, the solution was centrifuged at 9,000 rpm for 10 min to collect the precipitate, which was washed three times with distilled water. To remove residual salts and acids, the precipitate was dialysed using a dialysis tube (cut-off molecular weight of 12,000 Da) for at least 7 d by changing the water bath regularly (2 - 3 times per day), and the ACE-inhibitory activity of the sample was measured.

Cytotoxicity of RVPSL-GO

The cytotoxicity of RVPSL-GO was measured following a method previously reported with some modifications (Bassous and Webster, 2019). Hepatocytes were cultured in a 96-well plate (about 8,000 cells/well) with RPMI 1640 medium containing 10% foetal bovine serum 100 IU/mL penicillin and 100 mg/mL streptomycin. The RVPSL-GO solution was ultrasound treated for 30 min, and then mixed with a physiological solution. The solution was filtered with a filter membrane in an aseptic chamber. Hepatocytes (HepG2 cells) were washed three times with D-Hanks solution, and the cells were incubated with RVPSL-GO at final concentration of 100, 50, 10, 5, 1, 0.5, 0.1, and 0 µg/mL for different times (6, 12, 24, and 48 h) in a final volume of 100 µL medium; then, the medium was removed. Next, 100 µL of fresh medium and 20 µL of 3-(4,5-dimethylthiazol-2-yl)-5-(3-carboxymethoxyphenyl)-2-(4-sulfophenyl)-2H-tetrazolium (MTS) was added to each well, and the culture plates were incubated at 37°C with 5% CO₂ for 2 h. After removing of the medium, absorbance was measured at 492 nm using a microplate reader.

Results and discussion

Characterisation of RVPSL-GO

The elemental composition of the sample was

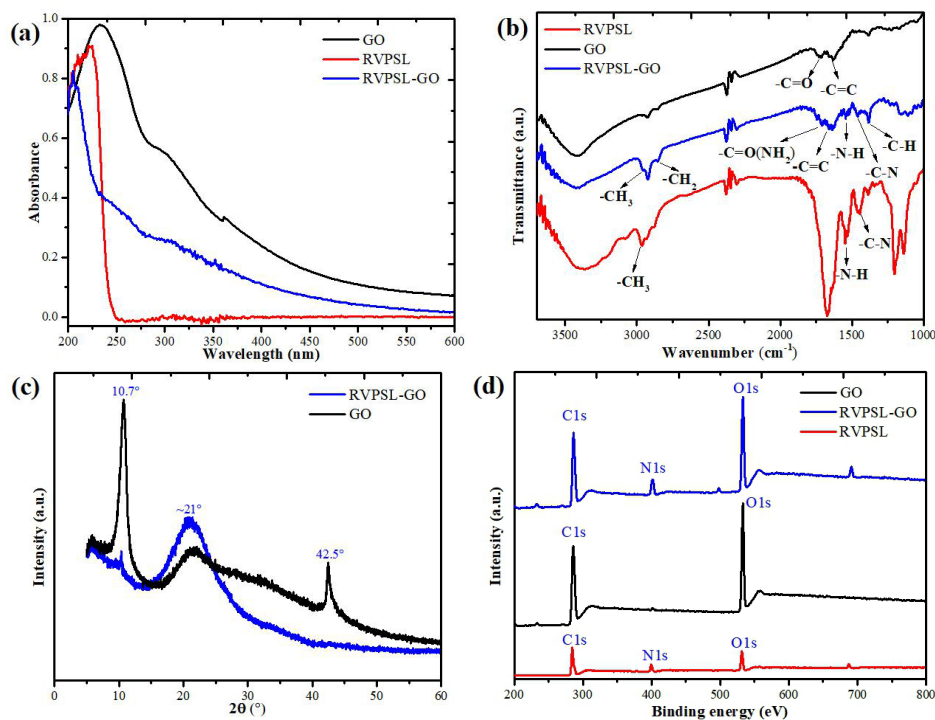


Figure 1. Structural characterisation of GO and RVPSL-GO by a variety of spectroscopic techniques: (a) UV-vis spectra; (b) FT-IR spectra; (c) XRD profile; and (d) XPS profiles. Pure GO sample was used as a reference system in order to reveal the changes in structures upon functionalisation.

investigated by UV-Vis absorption spectra and the structure of RVPSL-GO was precisely characterised. The results are shown in Figure 1a. The maximum RVPSL absorption peak emerged at 228 nm, which was the characteristic absorption peak of protein. The GO absorption peak was observed at 233 nm due to π - π^* transitions of C=C bonds, and a shoulder peak at 290 nm was attributed to n- π^* transitions of C=O bonds. The maximum RVPSL-GO absorption peak shifted to 205 nm due to the effect of the RVPSL functional groups. In addition, the shoulder peak at 303 nm also shifted, and a new peak was observed at 250 nm due to a reduction in the number of oxygen groups.

More detailed information about the RVPSL-GO chemical bonds was investigated using FT-IR. As shown in Figure 1b, three typical absorption bands were observed in the RVPSL spectrum at 1455, 1573, and 2954 cm^{-1} , which were from -C-N stretching, N-H bending, and -CH₃ asymmetric stretching, respectively. Four GO absorption peaks emerged at 1083, 1224, 1712, and 3466 cm^{-1} , which were from alkoxy C-O, epoxy C-O, C=O, and -OH stretching modes, respectively. The stretching frequency of C=O (1712 cm^{-1}) in RVPSL-GO shifted to 1654 cm^{-1} , and two new absorption peaks were observed at 1458 and 1570 cm^{-1} due to the C-N stretching and N-H bending, which were the characteristic of RVPSL absorption bands. Furthermore, a new peak at 2954 cm^{-1} from RVPSL-GO was attributed to asymmetric stretching of the RVPSL CH₃ groups. In addition, peaks at 1382 and 2924 cm^{-1} corresponded to the C-H stretching and bending were profound.

The RVPSL-GO XRD pattern is displayed in Figure 1c. A sharp GO peak was detected at the 2θ value of 10.74° (d-spacing: 0.83 nm). The large interlayer distance was attributed to the formation of hydroxyl, epoxy, and carboxyl groups between the GO layers. Another peak appeared at the 2θ value of 42.5° due to the turbostratic band of the disordered carbon materials (Chen *et al.*, 2011), which decreased following functionalisation. Furthermore, a broad peak was present at the 2θ value of 22.08° (d-spacing: 0.40 nm). The sharp peak was reduced as compared to GO, and a stronger peak was observed at the 2θ value of 21.4° (d-spacing: 0.41 nm) in the RVPSL-GO spectra.

The efficiency of RVPSL-GO was further estimated using XPS. As depicted in Figure 1d, both peaks of C1s at 284 eV and O1s at 531 eV appeared in the RVPSL, GO, and RVPSL-GO spectra. The N1s peak at 399 eV, which belonged to RVPSL, was also observed in RVPSL-GO. Moreover, three peaks at

284.6, 286.7, and 288.3 eV were observed in the de-convoluted RVPSL C1s XPS spectra of (Figure 2c), corresponding to C-C, C-O, and N-C=O groups, respectively. The RVPSL N1s spectrum was de-convoluted into two peaks at 399.3 eV for -NH- and 401.4 eV for free -NH₂ (Figure 2d). Furthermore, peaks of C-C/C=C, C-O, C=O/N-C=O, -NH-, and -NH₂ were observed in the de-convoluted RVPSL-GO C1s and N1s spectra, respectively (Figures 2e and 2f).

Morphology was measured by AFM and SEM. The thickness of a monolayer of graphene is ~0.34 nm (Gambhir *et al.*, 2015). The increased height of GO occurred because of the functional groups. The morphology of RVPSL-GO was characterised by AFM. The spectra (Figure 3) show the tapping mode of individual sheets of AFM images in more detail (Figure 3a, 3b) and together with the typical line profiles (Figures 3c and 3d) taken along the red line. Due to interactions between the cantilever, substrate, and nanosheets, the measured heights of the mono- or multilayers vary slightly (Walter *et al.*, 2015). As depicted in Figure 3d, the height of RVPSL-GO was about 2.5 nm. In Figure 3c, the height of GO was about 0.9 nm, which is similar to the previously reported values for a monolayer of GO (Ramesha and Sampath, 2009). The height change might occur due to the spatial structure of RVPSL and its chain length.

Subsequently, SEM was used to directly visualise the microstructure and elemental properties of the GO and RVPSL-GO surface. As shown in Figure 4, GO had an obvious 3-D structure, and the GO image showed a relatively rough film with a large surface area and size in Figure 4d. An immense number of wrinkles emerged on the surface of RVPSL-GO and a flaked structure was observed in the case of RVPSL-GO in Figure 4h, indicating low exfoliation of the nanosheets when RVPSL was covalently bonded to GO. As depicted in Figures 4e - 4g, the corresponding RVPSL-GO elemental mapping images were obtained including C, N, and O elements, further providing an evidence for covalent bonding of RVPSL. In conclusion, the peptide RVPSL was successfully covalently bonded to GO.

In vitro ACE-inhibitory activity of RVPSL-GO

The *in vitro* ACE-inhibitory activity of RVPSL-GO was measured to determine whether changes in the RVPSL structure affected the ACE-inhibitory activity of RVPSL. The ACE inhibition rate of RVPSL was 34.06% in concentrated S-RVPSL. The concentration of RVPSL in the S-RVPSL supernatant was 0.0054 mg/mL and the RVPSL-loading capacity of RVPSL-GO was calculated to be 1.05 mg RVPSL/mg GO, whereas the

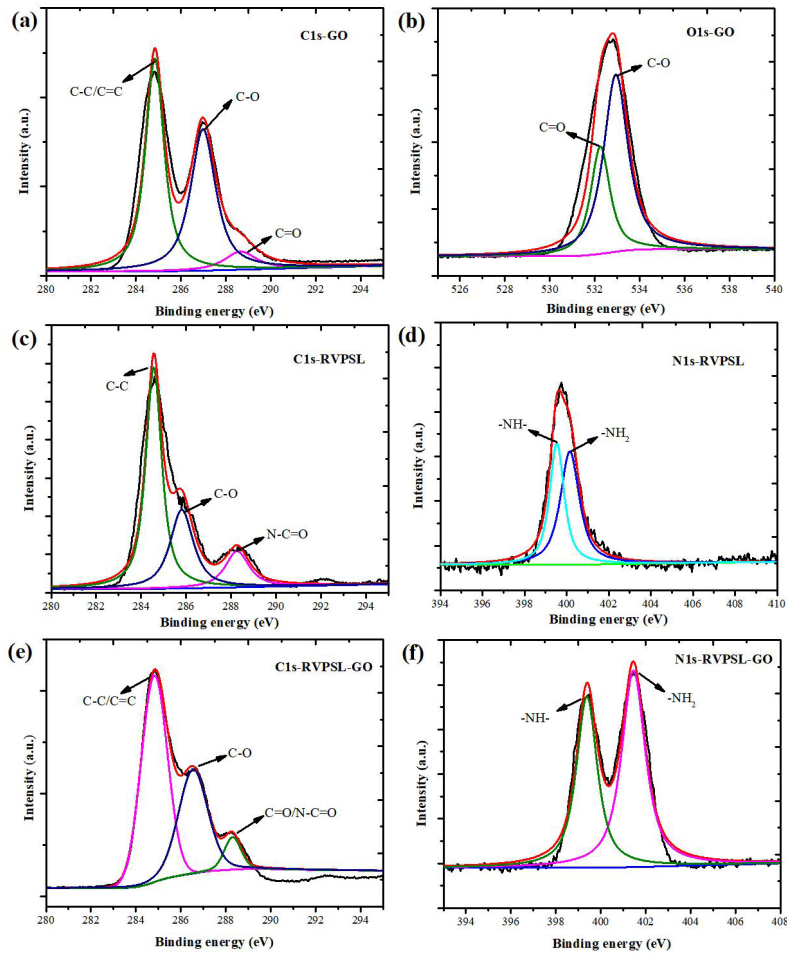


Figure 2. High-resolution de-convoluted spectra of RVPSL-GO and peptide RVPSL: (a) and (b) are the C1s and O1s of GO, respectively; (c) and (d) are the C1s and N1s of RVPSL, respectively; (e) and (f) are the C1s and N1s of RVPSL-GO, respectively.

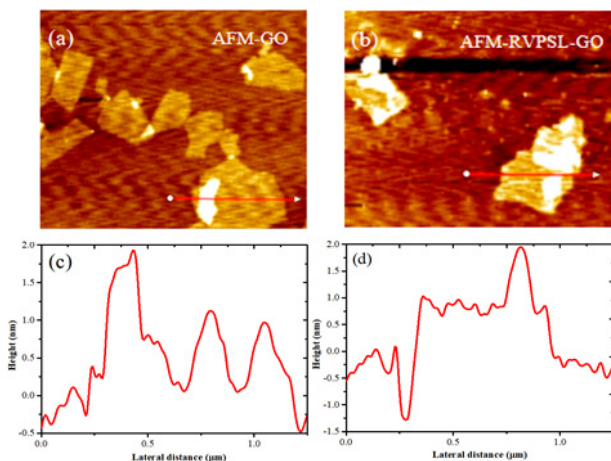


Figure 3. Detailed tapping mode AFM image: (a) the height images of GO and (b) the height images of RVPSL-GO. The line profiles in (c) and (d) were taken from the red lines marked in (a) and (b), respectively.

loading efficiency value was 95.02%. The ACE inhibition rate of RVPSL-GO increased from 26.47 to 39.70% at 0.05 mg/mL RVPSL, which was 1.5-fold of RVPSL without GO. The GO carboxylic acid

(-COOH) groups covalently bonded to the peptide RVPSL which may have caused a higher local concentration of RVPSL in the solution. The enhancement of ACE-inhibitory activity of the peptide RVPSL may have occurred with the change in its spatial structure. It has been reported that bioactive peptides bonded to nanomaterials enhance peptide activity. A 37-amino-acid native peptide, oxyntomodulin (Oxm) was converted into nanofibrils at a 94% conversion rate, and the activity of fibrillar Oxm was improved due to the formation of small size nanofibrillar structures (Ouberai *et al.*, 2017).

The stability of RVPSL-GO after gastrointestinal digestion

The peptide RVPSL was subjected to simulated proteolysis using the digestive proteases pepsin (EC 3.4.23.1) and trypsin (EC 3.4.21.4) in the online program ExPASy PeptideCutter (http://web.expasy.org/peptide_cutter/) (Yu *et al.*, 2020). The results revealed one trypsin restriction site between the amino acid residue Arg and a Val residue, thus indicating that RVPSL can be digested with trypsin. Subsequently, the GI digestion experiment was

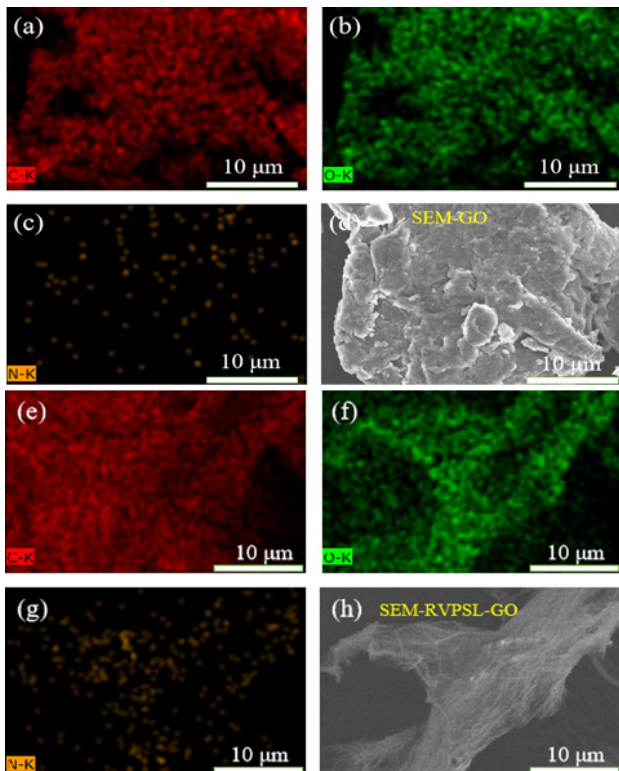


Figure 4. SEM and the elemental mapping images of GO and RVPSL-GO: (a-c) and (e-g) are the elemental mapping images of C, N, and O from GO and RVPSL-GO, respectively; (d) SEM image of GO; (h) SEM image of RVPSL-GO drop-casted on screen-printed electrode surface.

performed to determine if GO improved the stability of the peptide RVPSL in the GI tract. The RVPSL ACE inhibition rate was 22.92% after 1 h of simulated GI digestion, whereas the ACE inhibition rate of RVPSL-GO was 65.40% during the same digestion time. Then the peptide RVPSL degraded completely after 2 h of simulated GI digestion, and the ACE inhibition rate of RVPSL-GO was 49.08%, which was due to the GO structure protecting peptide RVPSL from degradation in the GI tract. The RVPSL-GO inhibitory percentage improved to 42.48% after 1 h of simulated GI digestion as compared to RVPSL. Furthermore, a 4 h GI digestion experiment was performed to further verify the protective ability of GO as a nano-material. As expected, the RVPSL-GO ACE-inhibitory rate was 29.56%, and RVPSL-GO did not completely degrade. These results indicate that GO enhanced the stability of RVPSL in a GI tract environment.

Cytotoxicity of RVPSL-GO

In the present work, the cytotoxicity of RVPSL-GO was examined using MTS and HepG2 cells. The effect of RVPSL-GO on HepG2 cells viability is illustrated in Figure 5. RVPSL-GO did not

induce obvious loss of viability ($\sim 10\%$) at 100 $\mu\text{g}/\text{mL}$. All cells reached 90% confluence in various incubation times in response to 100 $\mu\text{g}/\text{mL}$ RVPSL-GO. The RVPSL-GO was slightly toxic, as it damaged some cell membranes (low cell mortality) and inhibited cell growth. These results indicate that RVPSL-GO displayed good biocompatibility with HepG2 cells.

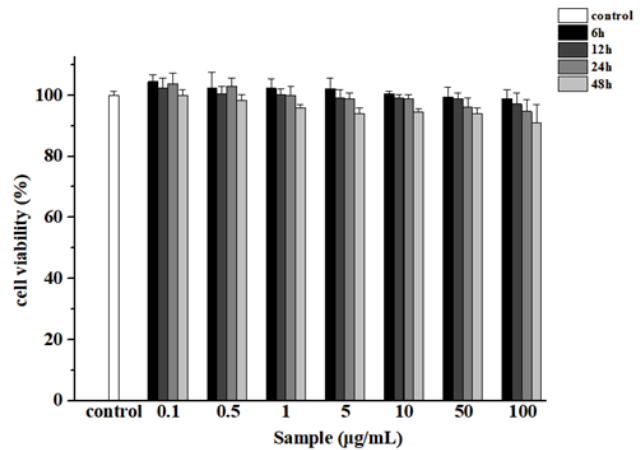


Figure 5. Cytotoxicity of sample (RVPSL-GO) particles to HepG2 cells after various incubation durations (6, 12, 24, and 48 h) and various concentrations (0, 0.1, 0.5, 1, 5, 10, 50, and 100 $\mu\text{g}/\text{mL}$).

Conclusion

In the present work, RVPSL-GO was successfully synthesised with a loading efficiency of 95.02%, and the RVPSL-loading capacity of RVPSL-GO was calculated to be 1.05 mg RVPSL/mg GO. RVPSL-GO exhibited 39.70% ACE inhibitory activity at 0.026 mg/mL. RVPSL was degraded completely after 2 h of simulated GI digestion, but RVPSL-GO retained an ACE inhibition rate of 49.08%. Moreover, RVPSL-GO exhibited high viability for HepG2 cells with no significant cytotoxicity. Based on these results, the ACE-inhibitory activity and stability of the peptide RVPSL were enhanced and protected by GO. The *in vivo* antihypertensive activity of RVPSL-GO needs to be evaluated in a further study.

Acknowledgement

The present work was financially supported by the National Key Research and Development Program of China (2018YFD0400301). The authors would also like to acknowledge Xinjiang Natural Science Foundation (No. 2018D01C040) and the research start-up fund of Xinjiang University (No. 4305050102H6).

References

- Ainslie, K. M., Lowe, R. D., Beaudette, T. T., Petty, L., Bachelder, E. M. and Desai, T. A. 2009. Microfabricated devices for enhanced bioadhesive drug delivery: attachment to and small-molecule release through a cell monolayer under flow. *Small* 5(24): 2857-2863.
- Bassous, N. J. and Webster, T. J. 2019. The binary effect on methicillin-resistant *Staphylococcus aureus* of polymeric nanovesicles appended by proline-rich amino acid sequences and inorganic nanoparticles. *Small* 15(18): article ID 1804247.
- Cabezas, E. and Satterthwait, A. C. 1999. The hydrogen bond mimic approach: solid-phase synthesis of a peptide stabilized as an α -helix with a hydrazone link. *Journal of the American Chemical Society* 121(16): 3862-3875.
- Chen, L., Xu, Z., Li, J., Min, C., Liu, L., Song, X., ... and Meng, X. 2011. Reduction and disorder in graphene oxide induced by electron-beam irradiation. *Materials Letters* 65(8): 1229-1230.
- Fasan, R., Dias, R. L. A., Moehle, K., Zerbe, O., Vrijbloed, J. W., Obrecht, D. and Robinson, J. A. 2004. Using a β -hairpin to mimic an α -helix: cyclic peptidomimetic inhibitors of the p53-HDM2 protein-protein interaction. *Angewandte Chemie* 43(16): 2109-2112.
- Gambhir, S., Jalili, R., Officer, D. L. and Wallace, G. G. 2015. Chemically converted graphene: scalable chemistries to enable processing and fabrication. *NPG Asia Materials* 7: article ID e186.
- Guarnieri, D., Sanchez-Moreno, P., Castillo, A. E. D. R., Bonaccorso, F., Gatto, F., Bardi, G., ... and Pompa, P. P. 2018. Biotransformation and biological interaction of graphene and graphene oxide during simulated oral ingestion. *Small* 14(24): article ID e1800227.
- Han, Y., Gao, Z., Chen, L., Kang, L., Huang, W., Jin, M., ... and Bae, Y. H. 2019. Multifunctional oral delivery systems for enhanced bioavailability of therapeutic peptides/proteins. *Acta Pharmaceutica Sinica B* 9(5): 902-922.
- Hirata, M., Gotou, T. and Ohba, M. 2005. Thin-film particles of graphite oxide. 2: preliminary studies for internal micro fabrication of single particle and carbonaceous electronic circuits. *Carbon* 43(3): 503-510.
- Hu, J.-J., Xiao, D. and Zhang, X.-Z. 2016. Advances in peptide functionalization on mesoporous silica nanoparticles for controlled drug release. *Small* 12(25): 3344-3359.
- Li, C., Dai, J., Zheng, D., Zhao, J., Tao, Y., Lei, J., ... and Liu, J. 2019. An efficient prodrug-based nanoscale delivery platform constructed by water soluble eight-arm-polyethylene glycol-diosgenin conjugate. *Materials Science and Engineering C* 98: 153-160.
- Martins, J. P., D'Auria, R., Liu, D., Fontana, F., Ferreira, M. P. A., Correia, A., ... and Santos, H. A. 2018. Engineered multifunctional albumin-decorated porous silicon nanoparticles for FcRn translocation of insulin. *Small* 14(27): article ID e1800462.
- Ouberai, M. M., Dos Santos, A. L. G., Kinna, S., Madalli, S., Hornigold, D. C., Baker, D., ... and Welland, M. E. 2017. Controlling the bioactivity of a peptide hormone *in vivo* by reversible self-assembly. *Nature Communications* 8: article no. 1026.
- Ramesha, G. K. and Sampath, S. 2009. Electrochemical reduction of oriented graphene oxide films: an *in situ* Raman spectroelectrochemical study. *Journal of Physical Chemistry C* 113(19): 7985-7989.
- Schafmeister, C. E., Po, J. and Verdine, G. L. 2000. An all-hydrocarbon cross-linking system for enhancing the helicity and metabolic stability of peptides. *Journal of the American Chemical Society* 122(24): 5891-5892.
- Shim, S. Y., Kim, Y.-W. and Verdine, G. L. 2013. A new i, i+3 peptide stapling system for α -helix stabilization. *Chemical Biology and Drug Design* 82(6): 635-642.
- Stankovich, S., Dikin, D. A., Dommett, G. H. B., Kohlhaas, K. M., Zimney, E. J., Stach, E. A., ... and Ruoff, R. S. 2006. Graphene-based composite materials. *Nature* 442: 282-286.
- Szabó, T., Tombácz, E., Illés, E. and Dékány, I. 2006. Enhanced acidity and pH-dependent surface charge characterization of successively oxidized graphite oxides. *Carbon* 44(3): 537-545.
- Tsomaia, N. 2015. Peptide therapeutics: targeting the undruggable space. *European Journal of Medicinal Chemistry* 94: 459-470.
- Vermeirssen, V., Van Camp, J. and Verstraete, W. 2004. Bioavailability of angiotensin I converting enzyme inhibitory peptides. *British Journal of Nutrition* 92(3): 357-366.
- Villar, E. A., Beglov, D., Chennamadhavuni, S., Porco, J. A., Kozakov, D., Vajda, S. and Whitty, A. 2014. How proteins bind macrocycles. *Nature Chemical Biology* 10(9): 723-731.
- Walter, J., Nacken, T. J., Damm, C., Thajudeen, T., Eigler, S. and Peukert, W. 2015. Determination of the lateral dimension of graphene oxide

- nanosheets using analytical ultracentrifugation. *Small* 11(7): 814-825.
- Wang, J., Yadav, V., Smart, A. L., Tajiri, S. and Basit, A. W. 2015. Stability of peptide drugs in the colon. *European Journal of Pharmaceutical Sciences* 78: 31-36.
- Yu, Z., Chen, Y., Zhao, W., Zheng, F., Ding, L. and Liu, J. 2019. Novel ACE inhibitory tripeptides from ovotransferrin using bioinformatics and peptidomics approaches. *Scientific Reports* 9(1): article ID 17434.
- Yu, Z., Ji, H., Shen, J., Kan, R., Zhao, W., Li, J., ... and Liu, J. 2020. Identification and molecular docking study of fish roe-derived peptides as potent BACE 1, AChE, and BChE inhibitors. *Food and Function* 11(7): 6643-6651.
- Yu, Z., Yin, Y., Zhao, W., Wang, F., Yu, Y., Liu, B., ... and Chen, F. 2011. Characterization of ACE-inhibitory peptide associated with antioxidant and anticoagulation properties. *Journal of Food Science* 76(8): C1149-C1155.
- Yu, Z., Zhao, W., Ding, L., Yu, Y. and Liu, J. 2016. Anxiolytic effects of ACE inhibitory peptides on the behavior of rats in an elevated plus-maze. *Food and Function* 7(1): 491-497.
- Yu, Z., Wu, S., Zhao, W., Ding, L., Shiuan, D., Chen, F., ... and Liu, J. 2018. Identification and the molecular mechanism of a novel myosin-derived ACE inhibitory peptide. *Food and Function* 9(1): 364-370.
- Zhao, W., Zhang, D., Yu, Z., Ding, L. and Liu, J. 2020. Novel membrane peptidase inhibitory peptides with activity against angiotensin converting enzyme and dipeptidyl peptidase IV identified from hen eggs. *Journal of Functional Foods* 64: article ID 103649.